

Eulerian-Lagrangian Solution of the Vertically Averaged Groundwater Transport Equation

L. R. BENTLEY

Department of Geology and Geophysics, University of Calgary, Calgary, Alberta, Canada

G. F. PINDER

College of Engineering and Mathematics, University of Vermont, Burlington

Eulerian-Lagrangian methods (ELMs) have been developed to reduce smearing and oscillations in numerically generated advection-dominated transport solutions. Improvements in front propagation characteristics are gained, but new sources of errors are introduced in the tracking step of ELMs. The Eulerian-Lagrangian least squares collocation method (ELLESCO) is applied to the vertically averaged transport equation, and the ELLESCO method is used to demonstrate how different types of discretization errors affect ELM solutions. The accuracy of ELMs is partially dependent on the accuracy of a tracking step. The tracking integration can be made as accurate as desired by dynamically adjusting the number of second-order Runge-Kutta integration steps per finite difference transport step. However, the accuracy of the final position is dependent on accurate velocities. Inaccurate velocities can lead to poorly located concentration fronts and mass balance errors. Although ELLESCO can extend the spatial and temporal discretization limits of classical methods, concentration fronts must be spread over one and a half elements to avoid oscillations in the solution. Time truncation errors associated with concentration dependent source terms lead to mass balance errors, and source terms should be computed with the Crank-Nicolson approximation to avoid excessive truncation error. The size of the finite difference transport time step and the magnitude of the local velocity determine the distance between the head and foot of the particle back tracks. This distance, referred to as the Lagrangian spatial resolution, must be less than the characteristic length of areal sources, or distortions will occur in the concentration front. The limit on the Lagrangian spatial resolution is an effective limit on the transport finite difference time step size.

INTRODUCTION

When sharp fronts exist in regions of advective-dominated flow, classical finite element and finite difference solutions of the transport equation are plagued with oscillations or numerical damping [Pinder and Gray, 1977]. Eulerian-Lagrangian methods (ELMs) have been developed to reduce these problems. A variety of ELMs have been shown to be effective in advective-dominated transport problems, but most applications have been limited to surface water transport of plumes [Baptista *et al.*, 1984; Cheng *et al.*, 1984; Glass and Rodi, 1982; Holly and Usseglio-Polatera, 1984; Komatsu *et al.*, 1985; Neuman, 1984; Zihuhua and Elsworth, 1989]. Applications to groundwater problems are limited, and those that exist have ignored the existence of areal source terms [Bentley and Pinder, 1992; Chiang *et al.*, 1989]. In this paper, some of the practical details of applying ELMs to areal groundwater flow problems will be discussed.

ELMs are attractive because they can be used with coarser spatial and temporal discretizations than classical methods when advection dominates dispersion in the transport equation. However, the tracking step of ELMs introduces sources of discretization errors that do not exist in classical methods. These discretization errors will be demonstrated and analyzed heuristically in the sections which follow. Although many of the points that will be made are applicable in general to ELMs, the discussion will be centered on the Eulerian-Lagrangian least squares collocation

method (ELLESCO). Development and error analysis of ELLESCO, as well as a comparison with other methods, can be found in the works by Bentley *et al.* [1989, 1990] and Bentley and Pinder [1992].

In the following, a brief review of the development of the ELLESCO system of algebraic equations is followed by a discussion on tracking and the presentation of a tracking algorithm. Example calculations are then used to demonstrate the consequences of certain discretization errors. Discussion is limited to steady state flow systems.

ELLESCO AND THE VERTICALLY AVERAGED TRANSPORT EQUATION

The vertically averaged flow and transport equations are often used in engineering applications. Given the following assumptions: (1) flow is saturated and steady, (2) porosity is time invariant, (3) fluctuations along the vertical of porosity are not correlated with the fluctuations of concentration, (4) no source-sink terms exist due to surface phenomena at the solid-water interface, chemical reactions or decay phenomena and (5) the dispersive flux across leakage boundaries is negligible, then the depth averaged transport equation can be written

$$\begin{aligned} \frac{\partial C}{\partial t} + V_x \frac{\partial C}{\partial x} + V_y \frac{\partial C}{\partial y} - \frac{1}{b\theta} \frac{\partial}{\partial x} \left(b\theta D_{xx} \frac{\partial C}{\partial x} + b\theta D_{xy} \frac{\partial C}{\partial y} \right) \\ - \frac{1}{b\theta} \frac{\partial}{\partial y} \left(b\theta D_{yx} \frac{\partial C}{\partial x} + b\theta D_{yy} \frac{\partial C}{\partial y} \right) \\ - (Q_a/b\theta) (C_a - C) - (Q_b/b\theta) (C_b - C) = 0, \quad (1) \end{aligned}$$

Copyright 1992 by the American Geophysical Union.

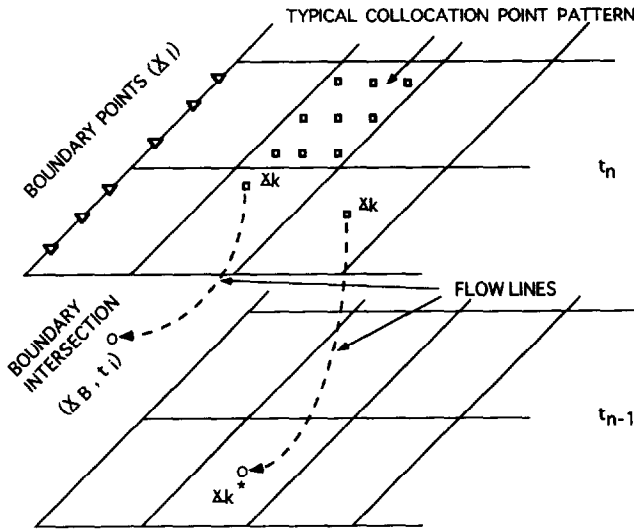


Fig. 1. ELLESCO discretization geometry. Collocation points from the time level in which the equation is being solved (squares) are tracked back along flow lines (dashed lines) until they intersect the last time level or domain boundary (circles). Penalty points (triangles) can be used to enforce boundary conditions.

where C is vertically averaged concentration, b is the layer thickness, θ is porosity, D_{ij} is an element of the dispersion tensor, Q_a and Q_b are fluid flux into the domain through the bottom and top boundaries respectively and C_a and C_b are the concentrations of those fluids. Equation (1) is now rewritten in Lagrangian form, and the fluid flux terms are replaced by expressions for leakage and infiltration:

$$\begin{aligned} \frac{DC}{Dt} - \frac{1}{b\theta} \frac{\partial}{\partial x} \left(b\theta D_{xx} \frac{\partial C}{\partial x} + b\theta D_{xy} \frac{\partial C}{\partial y} \right) \\ - \frac{1}{b\theta} \frac{\partial}{\partial y} \left(b\theta D_{yx} \frac{\partial C}{\partial x} + b\theta D_{yy} \frac{\partial C}{\partial y} \right) \\ + \frac{B}{b\theta} (\hat{h} - h_r)(C_L - C) - \frac{I}{b\theta} (C_I - C) = 0, \quad (2) \end{aligned}$$

where $D(\)/Dt$ is the substantial derivative, \hat{h} is a flow equation solution for vertically averaged head, h_r is a leakage reference head, B is the leakance parameter, I is infiltration, and C_L and C_I are the concentrations of the leakage and infiltrating fluids respectively. Point sources such as injection wells will be discussed in detail in the tracking section which follows.

A trial function is constructed with a cubic Hermite basis:

$$\hat{C} = \sum_{J=1}^{NJ} \alpha_J(t_n) \Phi_J(\mathbf{x}) \quad (3)$$

where NJ is the number of unknown coefficients $\alpha_J(t_n)$ and the functions $\Phi_J(\mathbf{x})$ are cubic Hermite polynomials.

The discretization of (2) follows the steps outlined by Bentley and Pinder [1992], and only a brief summary follows. Equation (2) is approximated by a finite difference in time directed along the flow lines which pass through individual collocation points (see Figure 1). This requires tracking back along the flow line which passes through the

collocation point to the position from which the flow line originated in the last time level, (x_k^*, y_k^*) . The trial function equation (3) is then substituted into the time-discretized form of (2). The resulting expression is evaluated at the individual collocation points, and after some rearrangement an expression for a collocation point residual can be written:

$$\begin{aligned} R_k = \sum_{J=1}^{NJ} \alpha_J \left[1 - \frac{\Theta \Delta t}{b\theta} \left(B(\hat{h} - h_r) - I + \frac{\partial}{\partial x} \left(b\theta D_{xx} \frac{\partial}{\partial x} \right. \right. \right. \\ \left. \left. \left. + b\theta D_{xy} \frac{\partial}{\partial y} \right) + \frac{\partial}{\partial y} \left(b\theta D_{yx} \frac{\partial}{\partial x} + b\theta D_{yy} \frac{\partial}{\partial y} \right) \right) \right] \Phi_{Jk} \\ - \left[\hat{C}_{k^*}^{n-1} - \frac{\Theta \Delta t}{b\theta} (BC_L(\hat{h} - h_r) - IC_I) \right] \\ - \frac{(1-\Theta)\Delta t}{b^*\theta^*} \left[\frac{\partial}{\partial x} \left(b^*\theta^* D_{xx}^* \frac{\partial \hat{C}_{k^*}^{n-1}}{\partial x} + b^*\theta^* D_{xy}^* \frac{\partial \hat{C}_{k^*}^{n-1}}{\partial y} \right) \right. \\ \left. + \frac{\partial}{\partial y} \left(b^*\theta^* D_{yx}^* \frac{\partial \hat{C}_{k^*}^{n-1}}{\partial x} + b^*\theta^* D_{yy}^* \frac{\partial \hat{C}_{k^*}^{n-1}}{\partial y} \right) \right] \\ - B^*(\hat{h}^* - h_r^*)(C_L^* - \hat{C}_{k^*}^{n-1}) + I^*(C_I^* - \hat{C}_{k^*}^{n-1}) \quad (4) \end{aligned}$$

where $\alpha_J = \alpha_J(t_n)$, $\Phi_{Jk} = \Phi_J(x_k, y_k)$, $\hat{C}_{k^*}^{n-1} = \sum_{J=1}^{NJ} \alpha_J(t_{n-1}) \Phi_J(x_k^*, y_k^*)$, parameters without asterisks are evaluated at the collocation point location, (x_k, y_k) , and parameters with asterisks are evaluated at the backtracked location, (x_k^*, y_k^*) . The time step size is Δt , and the parameter Θ is a time discretization weight. When $\Theta = 1$, the time discretization is implicit, and when $\Theta = 0.5$ the discretization is Crank-Nicolson.

Boundary condition residuals are specified at boundary penalty points, (x_i, y_i) :

$$R_i = \sum_{J=1}^{NJ} G \Phi_{Ji} \alpha_J - \bar{a}_i, \quad (5)$$

where G is an operator that represents the boundary condition and \bar{a}_i is the specified value of the boundary condition.

The individual collocation and boundary point residuals are squared, multiplied by a weight and then summed. The ELLESCO system of algebraic equations are formed by setting the derivatives of the weighted sums of squares with respect to each of the unknown coefficients, α_J to zero. If L and K denote the number of boundary points and collocation points respectively, and residual weights are denoted with W , then the system of equations can be written in matrix form as:

$$(\mathbf{A} + \mathbf{B})\boldsymbol{\alpha} = \mathbf{c} + \mathbf{d}, \quad (6a)$$

where

$$\begin{aligned} a_{iJ} = \sum_{k=1}^K W_k \left[1 - \frac{\Theta \Delta t}{b\theta} \left(B(\hat{h} - h_r) - I + \frac{\partial}{\partial x} \left(b\theta D_{xx} \frac{\partial}{\partial x} \right. \right. \right. \\ \left. \left. \left. + b\theta D_{xy} \frac{\partial}{\partial y} \right) + \frac{\partial}{\partial y} \left(b\theta D_{yx} \frac{\partial}{\partial x} + b\theta D_{yy} \frac{\partial}{\partial y} \right) \right) \right] \Phi_{Jk} \end{aligned}$$

$$\cdot \left[1 - \frac{\Theta \Delta t}{b\theta} \left(B(\hat{h} - h_r) - I + \frac{\partial}{\partial x} \left(b\theta D_{xx} \frac{\partial}{\partial x} + b\theta D_{xy} \frac{\partial}{\partial y} \right) + \frac{\partial}{\partial y} \left(b\theta D_{yx} \frac{\partial}{\partial x} + b\theta D_{yy} \frac{\partial}{\partial y} \right) \right) \right] \Phi_{Ik}, \quad (6b)$$

$$b_{IJ} = \sum_{l=1}^L W_l G \Phi_{Il} G \Phi_{Jl}, \quad (6c)$$

$$c_I = \sum_{k=1}^K W_k \left[\hat{C}_{k^*}^{n-1} - \frac{\Theta \Delta t}{b\theta} (BC_L(\hat{h} - h_r) - IC_I) + \frac{(1 - \Theta)\Delta t}{b^* \theta^*} \left(\frac{\partial}{\partial x} \left(b^* \theta^* D_{xx}^* \frac{\partial \hat{C}_{k^*}^{n-1}}{\partial x} + b^* \theta^* D_{xy}^* \frac{\partial \hat{C}_{k^*}^{n-1}}{\partial y} \right) + \frac{\partial}{\partial y} \left(b^* \theta^* D_{yx}^* \frac{\partial \hat{C}_{k^*}^{n-1}}{\partial x} + b^* \theta^* D_{yy}^* \frac{\partial \hat{C}_{k^*}^{n-1}}{\partial y} \right) - B^*(\hat{h}^* - h_r^*)(C_L^* - \hat{C}_{k^*}^{n-1}) + I^*(C_I^* - \hat{C}_{k^*}^{n-1}) \right) \right] \cdot \left[1 - \frac{\Theta \Delta t}{b\theta} \left(B(\hat{h} - h_r) - I + \frac{\partial}{\partial x} \left(b\theta D_{xx} \frac{\partial}{\partial x} + b\theta D_{xy} \frac{\partial}{\partial y} \right) + \frac{\partial}{\partial y} \left(b\theta D_{yx} \frac{\partial}{\partial x} + b\theta D_{yy} \frac{\partial}{\partial y} \right) \right) \right] \Phi_{Ik}, \quad (6d)$$

$$d_I = \sum_{l=1}^L W_l \bar{a}_l G \Phi_{Il}, \quad (6e)$$

and it is implied that $\Theta = 1$ and $\Delta t = \Delta t_i = t_n - t_i$ for collocation points whose tracks intersect the domain boundary at time t_i . The system matrix of (6) is symmetric positive definite.

NUMERICAL TRACKING

In ELLESCO, the backtracked location of each collocation point, x_k^* , is

$$x_k^*(t_{n-1}) = x_k + \int_{t_n}^{t_{n-1}} V(x(t)) dt. \quad (7)$$

Since the velocity field may be complicated, (7) is generally integrated numerically. The accuracy of the solution to (7) depends on the procedure used for the numerical integration, the size of the time steps used in the numerical integration and the local complexity of the velocity field. The discussion which follows assumes a steady state velocity field, and the complexities associated with time-varying flow fields are not herein discussed.

An advantage of ELMs is that the transport time step size can be large compared to classical methods. However, the accuracy of the ELM solution is dependent on the tracking error. Consequently, it is advantageous to decouple the integration time step size from the transport time step size in order to track as accurately as necessary without decreasing the transport time step size. In addition, in areas where the

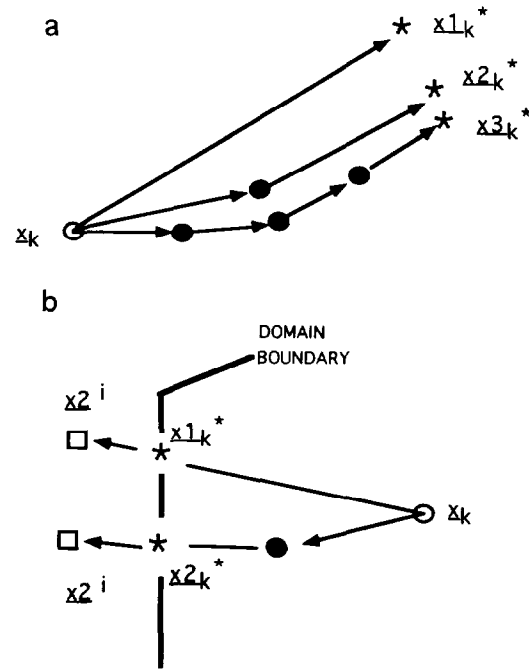


Fig. 2. Numerical tracking. (a) One-, two- and four-step second-order tracks. Open circle is the collocation point location. Solid circles are the second-order Runge-Kutta solutions and stars are the final tracking solutions. (b) Domain boundary intersection. Open squares are intermediate positions of the second-order Runge-Kutta algorithm. Stars indicate the final tracking solutions.

flow lines are curved, Euler or backward projection-based integrations lead to position errors that are consistently to the convex side of the flow path. These tracking errors tend to be additive, and second-order Runge-Kutta-based integrations have proven superior to Euler-based integrations.

Equation (7) is solved by a sequence of second-order Runge-Kutta integrations, each of which can be summarized by the following two steps:

$$x2^i = x1 - \Delta t_m V(x1), \quad (8a)$$

$$x2 = x1 - (V(x1) + V(x2^i)) \frac{\Delta t_m}{2}, \quad (8b)$$

where $x1$ is the starting position, $x2^i$ is an intermediate position, $V(x2^i)$ is the velocity at the intermediate position, Δt_m is the tracking time step interval and $x2$ is the new position. Each collocation point is tracked back individually, and the number of second-order Runge-Kutta steps per transport time step is adjusted to meet a spatial accuracy criterion.

First, the integration is done in one step, that is, $\Delta t_m = \Delta t$, $m = 1$. Then, the integration is done in two steps of $\Delta t_m = \Delta t/2$, $m = 1, 2$ (Figure 2a). The coordinate denoted xN_k^* is the coordinate of the numerical solution to (7) which used a series of second-order Runge-Kutta time steps of length $\Delta t_m = \Delta t/N$, $m = 1, 2, \dots, N$. The final position of the two solutions is compared. If the differences in the x and y coordinates of $x1_k^*$ and $x2_k^*$ are less than a user-specified tracking accuracy criterion, ϵ_m , the spatial accuracy of the tracking step is considered sufficient. The position of the more accurate two-step solution $x2_k^*$ is assigned to x_k^* , and the algorithm proceeds to the next collocation

point. If either of the coordinates does not meet the criterion, the integration is repeated using four steps of $\Delta t_m = \Delta t/4$, $m = 1, 2, 3, 4$ and the two-step and four-step solutions are compared. The tracking time step interval is halved in this manner until the spatial accuracy criterion is met, and \mathbf{x}_k^* is assigned the position of the solution which used the smallest integration time step interval. Experience has shown that a tracking criterion of one hundredth of the smallest element dimension is sufficient for ELLESCO. The procedure automatically adjusts to the local complexity of the velocity field and is efficient if there are a limited number of complex flow zones. The dynamic adjustment of Δt_m means that the time truncation errors associated with the advective step are limited in magnitude, and, most importantly, they are effectively independent of the size of the transport time step, Δt .

Similar logic is applied to the tracks that intersect the domain boundary (Figure 2b). A flow velocity does not exist for an intermediate position which falls outside of the domain boundary, and the second-order Runge-Kutta cannot be used for that integration interval. If an intermediate point is determined to be outside of the domain, the intersection of the appropriate straight line segment that approximates the domain boundary and the line segment connecting \mathbf{x}_1 and \mathbf{x}_2^i is found. The numerical solution to (7), $\mathbf{x}N_k^*$, is the location of the point of intersection. Then the boundary intersection coordinates of numerical integration solutions using different time step intervals are compared, and the tracking time step interval is decreased by halves until the spatial accuracy criterion is met.

A flow line which intersects the domain boundary does not spend an entire transport time step within the domain, and the length of the time step interval, Δt , in (6) should be adjusted to the length of time the flow line was in the domain, Δt_i . The time inside the domain can be approximated by multiplying the tracking step length, Δt_m , by the number of second-order Runge-Kutta steps and adding the amount of time spent in the truncated portion of the back projection.

VELOCITY SINGULARITIES AND INJECTION WELLS

Pumping and injection wells cause singularities in the two-dimensional velocity field. Since collocation points will track away from pumping wells, they pose no particular difficulties as long as the velocity field is reasonably well represented near the singularity. However, tracking back to the velocity singularity associated with an injection well is extremely difficult, and a special procedure is required.

An injection well is an internal boundary, and, hence, collocation points whose flow lines originated at the injection well during the transport time step are handled as if they intersected a domain boundary. The information that is required from the tracking step is the concentration at the backtracked location and the length of time a flow line was in the domain, Δt_i , during the transport time step. It is assumed that the concentration of the injected fluid is known. Accordingly, the injected fluid concentration is assigned to backtracked locations of all collocation points whose flow lines originate at the injection well. The problem reduces to finding the collocation points whose flow lines originate at the well and approximating the amount of time they were in the domain.

The approach is to track forward from the injection well.

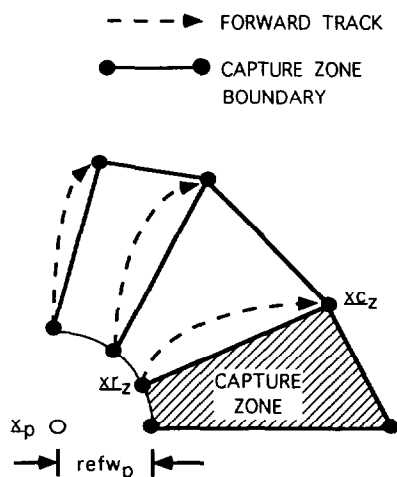


Fig. 3. Injection well capture zones. Dashed lines represent the forward tracks from the effective well perimeter. Solid lines connecting solid points are the resultant capture zones.

As shown in Figure 3, an effective well radius, r_{wef_p} , is set to one twentieth of the minimum dimension of the flow grid element that contains the well. Points along the effective well radius at locations, x_{r_z} , are tracked forward to the outer boundary of the capture zone, x_{c_z} , by

$$\mathbf{x}_{c_z} = \mathbf{x}_{r_z} + \int_{t_{n-1}}^{t_n} V(\mathbf{x}(t)) dt. \quad (9)$$

The integration is performed numerically using the procedure that was described for the backward integration. The coordinates x_{r_z} and x_{c_z} are used to define a set of quadrilateral capture zones as shown in Figure 3.

If the position of a collocation point, \mathbf{x}_k , is located in a capture zone, the backtracking step is skipped, and the collocation point is flagged as captured. Its backtracked concentration value is set to the value of the injected fluid, and an estimate of the length of time that the collocation point was in the domain during the time step is computed.

Since the injection wells represent internal boundaries, a constant concentration penalty residual, equation (5), can be applied at well locations. Numerical experiments show that the penalty residual is not necessary. Indeed, the use of a penalty residual often degrades the solution, because the penalty condition strongly enforces the spikelike concentration associated with initial conditions, causing strong Gibbs spatial oscillations at early time. Without the penalty residual, the initial concentration can grow somewhat more slowly, and the oscillations are less severe. Consequently, penalty residuals are not used at well locations.

ADVANCING FRONT FROM AN INJECTION WELL

When a fluid of constant concentration is injected into a homogeneous aquifer at a constant rate, a circular concentration front develops. An analytical solution exists for the case of an infinite homogeneous confined aquifer with homogeneous initial and boundary conditions [Javandel et al., 1984]. In the following, analytical solutions will be compared to implicit ($\Theta = 1$) ELLESCO solutions computed with the numerical tracking algorithm described in the previous section.

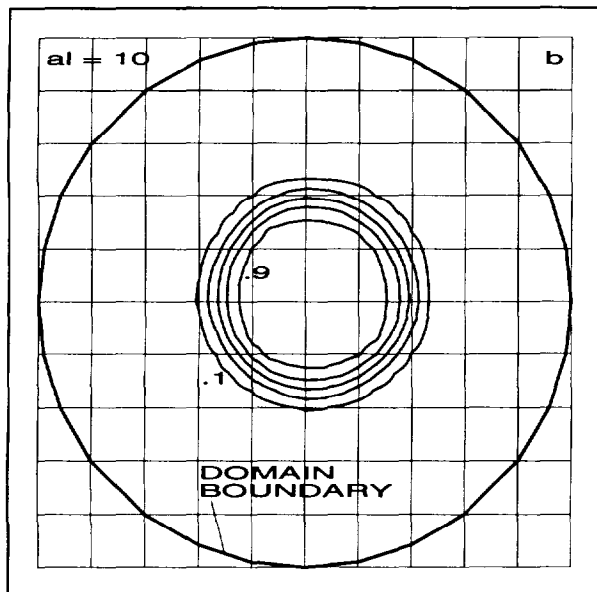
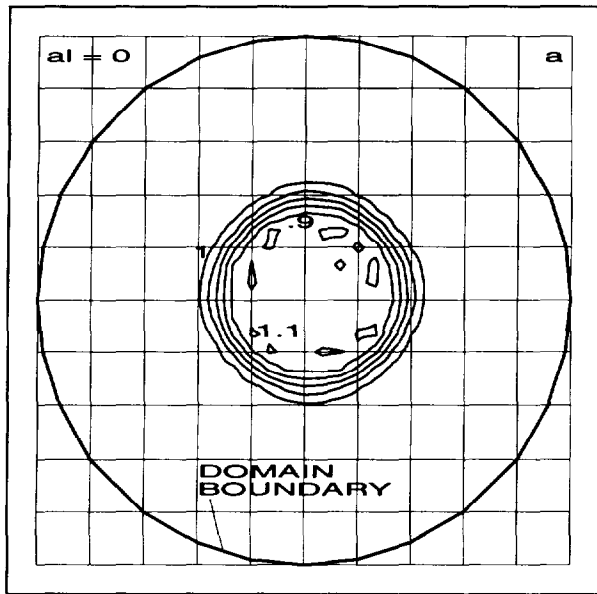


Fig. 4. Concentration contours, injection into a circular aquifer. ELLESCO-generated equal concentration contours after 15 time steps for longitudinal dispersivities of (a) zero and (b) $a_L = 10$ m. Contour interval is 0.2 m.

The calculations were performed using a coarse mesh with 200 m by 200 m elements (Figure 4). A nine-point rectangular collocation point pattern was used except in the center four elements near the source. As shown in Figure 5, the center four elements contain a radial pattern centered on the source location. The source location is located within an element, 25 m north and 25 m east of the grid center (see Figure 5). The tracking convergence criterion was 0.2 m. A zero normal derivative was imposed on the approximation to a circular boundary shown in Figure 4. Six penalty points per boundary element were used and the boundary weights, $W_i = 10^4$. Fifteen time steps of 10^8 s were calculated. The local Courant number varies from approximately 2.0 at the center of the grid, near the source, to less than 10^{-2} at the domain boundary.

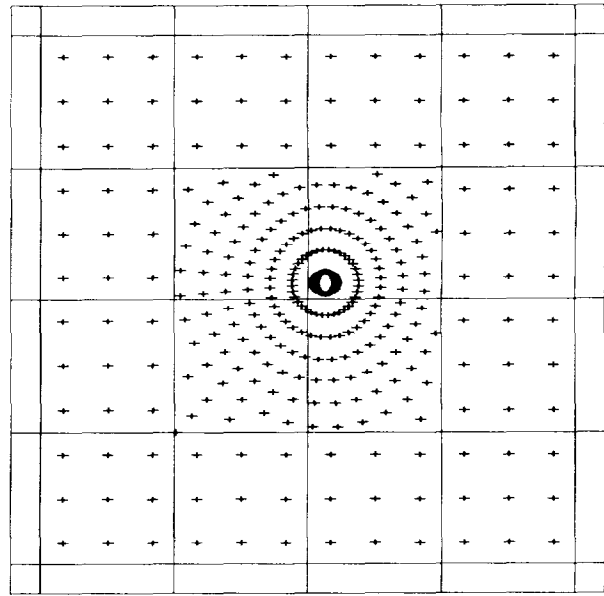


Fig. 5. Radial collocation point pattern, injection into a circular aquifer. In the four center elements, a radial collocation point pattern (pluses) is centered on the injection well location. The remainder of the domain has the nine-point pattern.

The first set of results were calculated with no dispersion. Contours of the final concentration field calculated with numerically generated velocities are found in Figure 4a. The circular plume is slightly off center, reflecting the nonsymmetric source location. The small contours interior to the plume are indicative of overshoot. The width of the front is somewhat less than one element length. Cross sections through the source striking 0° and 45° are presented in Figure 6 for results computed with analytical velocities (Figure 6a) and numerically generated velocities (Figure 6b). The form of the profiles of the two solutions is similar. Both profiles exhibit large oscillations and smeared fronts due to the coarseness of the grid. They both appear reasonably well located compared to the analytical solution. However, on close inspection, the numerical velocity result is slightly lagged relative to the analytical velocity result. The lagging is caused by errors in the numerically computed flux. The normalized mass is defined as the ratio of the computed mass in the system to the known injected mass. The normalized mass is one, less than one and greater than one for solutions with perfect mass balance, too little mass and too much mass respectively. The normalized mass at time steps 5, 10 and 15 is 1.022, 1.000 and 1.008, respectively, for the analytical velocity solution and 0.998, 0.964 and 0.961, respectively, for the numerical velocity solution.

A second set of results were calculated with a longitudinal dispersivity, $a_L = 10$ m, transverse dispersivity, $a_T = 0$ m and diffusion constant, $D_0 = 0$ m²/s. Contours of the final concentration field calculated with numerically generated velocities are found in Figure 4b. The circular plume is once again slightly off center, reflecting the nonsymmetric source location. The concentration front is slightly broader than the previous case, being approximately one element length across. Cross sections through the source striking 0° and 45° are presented in Figure 7 for results calculated with analytical velocities (Figure 7a) and numerical velocities (Figure

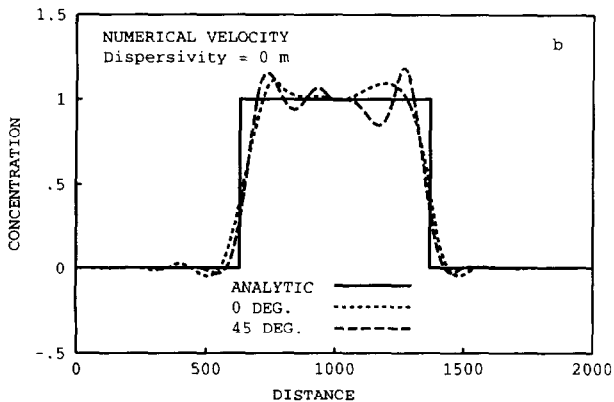
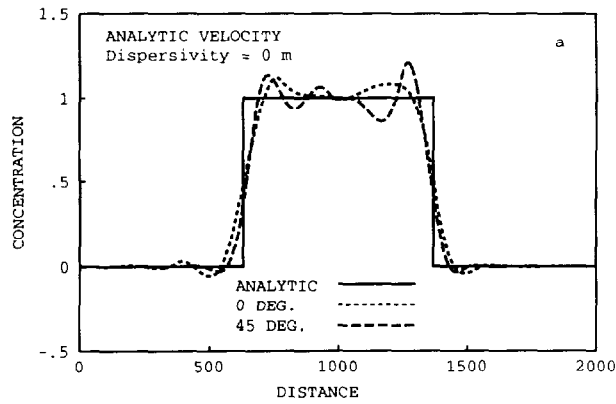


Fig. 6. Concentration profiles, injection into a circular aquifer. Concentration profiles through the injection well location are compared for the zero dispersivity case. ELLESCO results generated with (a) the analytical velocity field and (b) a numerical velocity field are compared to the analytical solution. ELLESCO profiles strike 0° and 45° .

7b). These two solutions are similar in form, and the oscillations have almost vanished. The shapes of the fronts closely match that of the analytical solution, but, once again, the numerical velocity-generated solution slightly lags the analytical velocity-generated solution. The normalized mass at time steps 5, 10 and 15 is 1.034, 1.012 and 1.012, respectively, for the analytical velocity solution and 1.037, 0.989 and 0.978, respectively, for the numerical velocity solution.

From the results we see that time steps that produce locally large Courant number can be used without adversely affecting the solution. When the front is broad enough, ELLESCO will accurately represent it. However, if the front is too narrow, the solution is contaminated with oscillations, demonstrating the resolution limit of the Eulerian grid. Consistent with Fourier analysis [Bentley et al., 1990], oscillations do not develop if the front is spread over at least one and one half elements. The results also demonstrate the obvious and important fact that the accuracy of the solution is limited by the accuracy of the velocity field used to generate it. Inaccurate velocities will cause the concentration front to be poorly located. In addition, the strength of the source is determined by the injection well flow rate, which enters the transport calculation through the tracking velocity. Consequently, ELLESCO can develop global mass balance errors if numerically computed velocities are inaccurate. When ELLESCO used the analytical velocities and

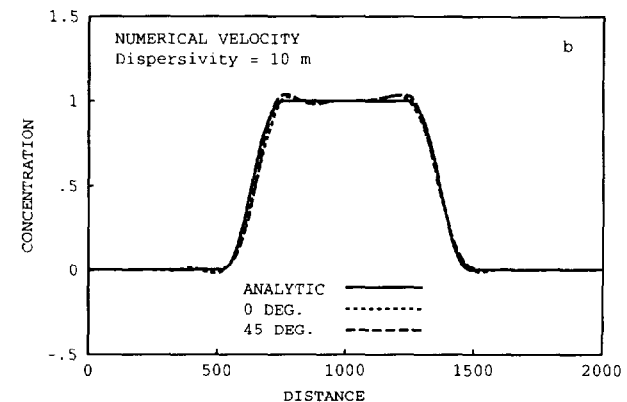
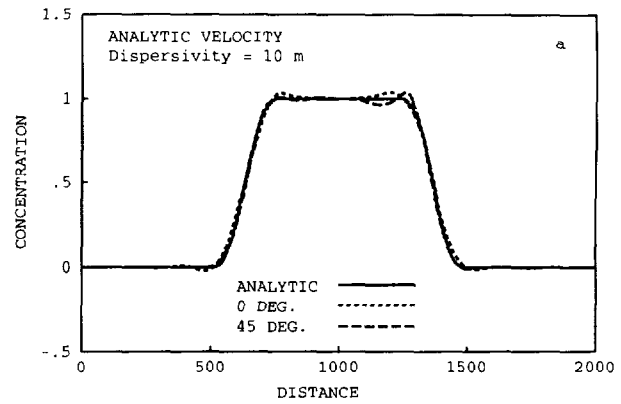


Fig. 7. Concentration profiles, injection into a circular aquifer. Concentration profiles through the injection well location are compared for the $a_1 = 10$ m case. ELLESCO results generated with (a) the analytical velocity field and (b) a numerical velocity field are compared to the analytical solution. ELLESCO profiles strike 0° and 45° .

accurate numerical tracking, mass balance errors were of the order of 1%, even when the solution was contaminated by serious oscillations. The flux errors in the numerically generated flow field caused mass balance errors of up to 4%.

RECHARGE THROUGH A CONTAMINATED SOIL

Infiltrating rainwater can become contaminated when passing through tainted soil as it travels through the unsaturated zone. A contaminant plume will develop in the area of contaminated recharge. The results in this section simulate contaminated recharge into a phreatic aquifer. The results are computed with the previously described tracking algorithm and they will demonstrate time discretization limits that arise in the presence of areal sources.

A square domain is inscribed on a rectangular grid constructed with elements of dimension 100 m by 100 m as shown in Figure 8. The flow system is that of a phreatic aquifer with uniform recharge over the domain. The no-flow boundary in the northeast represents a groundwater divide and the two no-flow boundaries in the northwest and southeast represent streamlines. The constant head boundary in the southwest represents a river. Groundwater flux and head profiles through the center of the aquifer starting at the no-flow boundary in the northeast and continuing to the constant head boundary in the southwest are presented in Figure 9. As seen in Figure 9, the magnitude of the flux in the example varies from zero at the groundwater divide in the

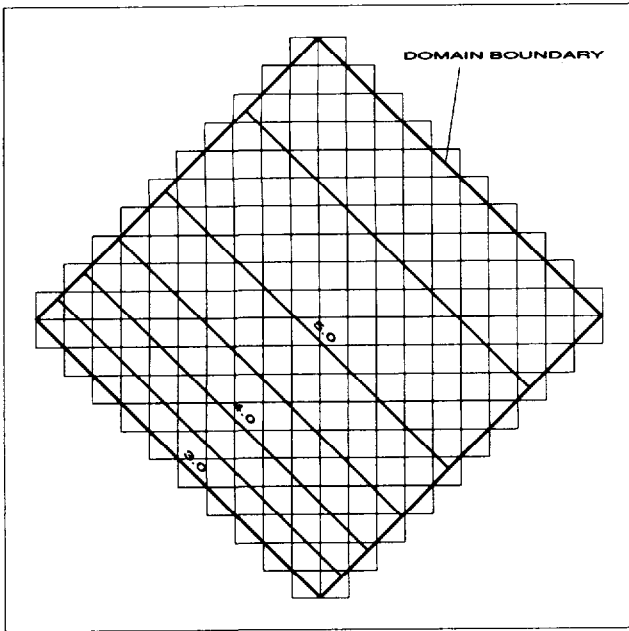


Fig. 8. Finite element mesh, contaminated soil problem. A square domain, rotated 45° relative to the grid orientation, is inscribed on an orthogonal mesh. Element dimensions are 100 m by 100 m. Heads are contoured at 0.5 m intervals.

northeast to $2.27 \times 10^{-6} \text{ m}^2/\text{s}$ at the river in the southwest. Head and aquifer thickness vary parabolically from 5.63 m in the northeast to 3.00 m in the southwest. The porosity of the aquifer is 0.40. The dispersivities and the diffusion constant are set to zero.

In this problem, the dispersion is zero, and the problem is hyperbolic. Formally, boundary conditions should only be applied on inflow boundaries of hyperbolic partial differential equations. All of the boundaries surrounding the horizontal extent of the domain are no-flow or outflow boundaries, and, consequently, no boundary penalty points are used. The tracking criterion was $\epsilon_t = 0.1 \text{ m}$.

Infiltration sources arise when the concentration of the recharge water, C_I , of (2) is nonzero. The concentration of the contaminated recharge water is an input parameter, and the concentration field is represented by a bilinear basis. Results from simulations using a one-node source and a four-node source (Figure 10) are presented. The one-node

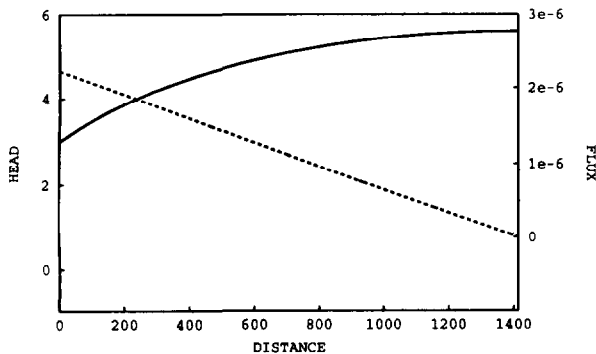


Fig. 9. Head and total flux profiles, contaminated soil problem. Heads (solid line) and total flux values (dashed line) are profiled along the centerline of the domain shown in Figure 8.

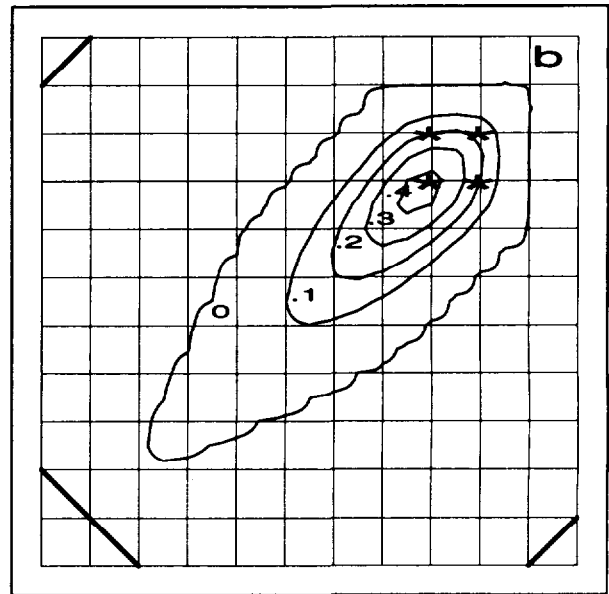
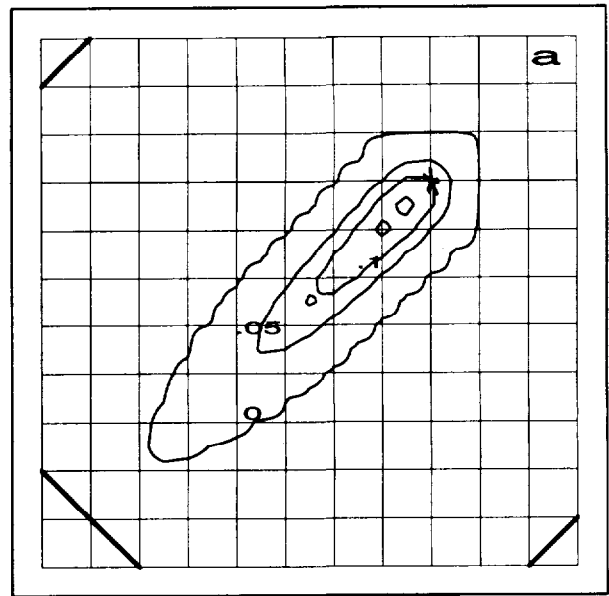


Fig. 10. Concentration contours, contaminated soil problem. Crank-Nicolson ELLESCO results using time step increment $\Delta t = 4$ years are contoured at time 32 years for (a) the one-node source and (b) the four-node source. Stars indicate source nodes and heavy lines are domain boundaries.

source infiltration concentration is pyramidal, with a value of $C_I = 1$ at the source node and tapering to zero at the outer perimeter of the four elements surrounding the source node. The four-node source infiltration concentration appears as a truncated pyramid, with the central element at $C_I = 1$ and tapering to zero along the perimeter of a nine-element square. As contaminant enters the domain, a plume develops. Generally, concentrations increase with time as more contaminant is introduced. Even in the absence of dispersion, concentrations decrease downgradient of the source area, because clean water is recharging into the plume downgradient of the source.

All simulations were carried out to a total time of 32 years. Dispersivities were set to zero. Final concentration contours

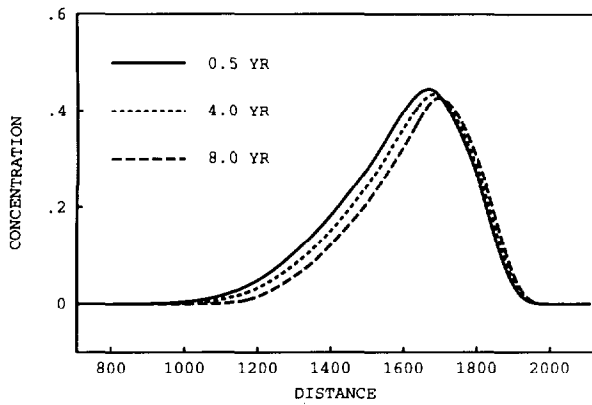


Fig. 11. Concentration profiles, contaminated soil problem. Concentration profiles along the streamline that passes through the center of the four-node source are plotted for implicit solutions at time 32 years with time step increments $\Delta t = 0.5$ year ($Co = 0.035$), $\Delta t = 4$ years ($Co = 0.28$) and $\Delta t = 8$ years ($Co = 0.56$).

of representative solutions for the two sources are presented in Figure 10. An analytical solution to this problem does not exist. However, the theoretical value of the mass that has entered the system is known, and the normalized mass is used as one measure of accuracy.

The four-node source example was simulated with implicit ($\Theta = 1$) ELLESCO and a variety of time step intervals. Concentration profiles along the streamline passing through the center of the source are presented in Figure 11. The normalized mass versus time step size is shown in Figure 12. The implicit version of ELLESCO consistently underpredicts the mass, and the error increases almost linearly with the time step interval, consistent with a first-order time truncation error. An effect of the time truncation error is to create mass errors greater than 1% for time steps of a year or greater. This corresponds to a Courant number at the source location of 0.07, which is an extreme restriction on the time discretization. (All Courant numbers quoted in this section are computed at the source.)

The underprediction of mass can be understood by examining the form of the source term in (2). The magnitude of the source is proportional to $(C_I - C)$. The implicit formulation approximates C by the forward time level trial function \hat{C}^n .

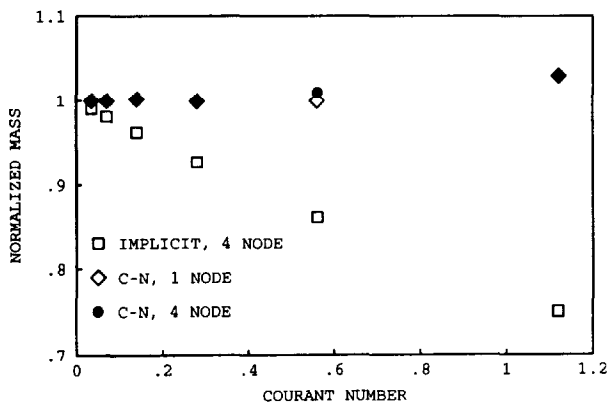


Fig. 12. Normalized mass versus Courant number. The normalized mass at time 32 years is plotted for implicit solutions of the four-node source. Crank-Nicolson solutions of the four-node source and Crank-Nicolson solutions of the one-node source.

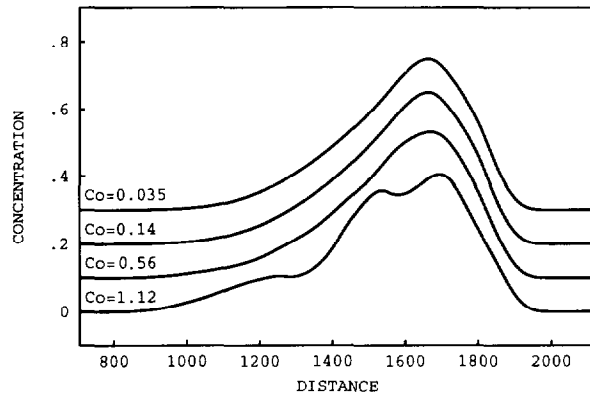


Fig. 13. Concentration profiles, contaminated soil problem. Concentration profiles along the streamline that passes through the center of a four-node source are shown for four Crank-Nicolson solutions at time 32 years. Starting at the top, time step increments were $\Delta t = 0.5$ year ($Co = 0.035$), $\Delta t = 2$ years ($Co = 0.14$), $\Delta t = 8$ years ($Co = 0.56$) and $\Delta t = 16$ years ($Co = 1.12$).

Since C is growing with time, \hat{C}^n is the largest value that will exist in the closed time interval of $[t_{n-1}, t_n]$. Consequently, the approximation $(C_I - \hat{C}^n)$ is always the lower bound of an approximation that should be computed with an integral average of C .

The four-node source example was also simulated with ELLESCO using a Crank-Nicolson formulation ($\Theta = 0.5$). Concentration profiles along the streamline passing through the center of the source are presented in Figure 13, and the normalized mass in Figure 12. The benefits of the higher-order time approximation are evident in the mass balance. Mass is conserved to better than 1% at $\Delta t = 8$ years ($Co = 0.56$). At $\Delta t = 16$ years ($Co = 1.12$), a 3% mass error has developed.

Figure 14 shows a comparison of implicit and Crank-Nicolson solutions for time step intervals $\Delta t = 0.5$ year and $\Delta t = 8$ years. The $\Delta t = 0.5$ year solutions are almost identical, demonstrating that the Crank-Nicolson and implicit solutions converge to the same solution as the magni-

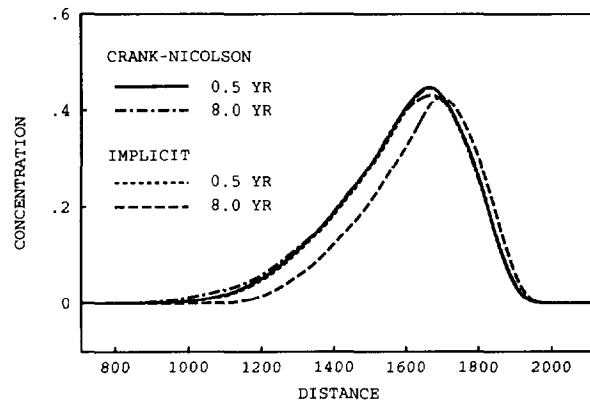


Fig. 14. Comparison of implicit and Crank-Nicolson solutions. Concentration profiles along the streamline that passes through the center of a four-node source at time 32 years are shown for Crank-Nicolson solutions computed with time step increments $\Delta t = 0.5$ year ($Co = 0.035$) and $\Delta t = 8$ years ($Co = 0.56$) and for implicit solutions computed with time-stepping increments of $\Delta t = 0.5$ year ($Co = 0.035$) and $\Delta t = 8$ years ($Co = 0.56$).

tude of Δt decreases. The Crank-Nicolson solution using $\Delta t = 8$ years is only slightly dispersed and has a mass error of less than 1%. In contrast, the implicit solution using $\Delta t = 8$ years is significantly lagged and has a 14% mass error.

Profiles presented in Figure 13 show that the Crank-Nicolson solution is only slightly dispersed at $Co = 0.56$ (see also Figure 14). However, at $Co = 1.12$, serious distortions of the front begin to appear. These distortions, which are not present in classical Eulerian methods, are manifestations of a Lagrangian spatial resolution effect. They arise because the substantial derivative is approximated by a finite difference in time along the streamlines of the flow field. The time discretization is inherently tied to spatial resolution through the distance that separates the head and the foot of the characteristics. A local measure of the Lagrangian spatial resolution is $V\Delta t$. The Lagrangian spatial resolution can be related to the Eulerian spatial discretization through the dimensionless Courant number:

$$\Delta x_L = V\Delta t = Co\Delta x. \quad (10)$$

The Lagrangian spatial resolution is a function of the time step or, alternatively, the Courant number.

As Δx_L becomes large compared to the areal dimension of geographically fixed features, the approximation to the substantial derivative deteriorates. As an extreme example, consider a collocation point that is located outside of a source area. Further, assume that it tracks across the source area to a location on the opposite side of the source. The collocation point residual, equation (4), would have no forcing due to the source. However, collocation points upstream and downstream would terminate or originate in the source area, and, consequently, they would have forcing terms in their residuals. As a result, the source area would be represented as a double-humped feature. The bottom profile of Figure 13 exhibits the beginnings of such a feature. In order to preserve the character of the sources, the magnitude of the Lagrangian spatial resolution parameter, Δx_L , must be smaller than the characteristic length of a source in the region of the source.

The time step interval is therefore limited by time truncation errors and by limits on the local Courant number through limits on Δx_L . In the examples in this section, the time truncation errors cause mass errors. The Lagrangian spatial resolution errors appear as distortions in the front. Smaller features place greater constraints on Δx_L , and consequently the time step interval, than larger features.

To illustrate, a one-node source example was solved with ELLESCO using a Crank-Nicolson time approximation (Figure 10). Again, the total time of simulation is 32 years. Figure 15 shows profiles along the streamline passing through the source node for a variety of time step intervals, and Figure 12 displays the mass balance results. Mass balance results are almost identical to those of the four-node Crank-Nicolson example, indicating that the time truncation errors are independent of the source size. However, the results from the narrow source example show the beginnings of distortions at $\Delta t = 8$ years ($Co = 0.56$), and they are severely distorted at $\Delta t = 16$ years ($Co = 1.12$). Comparing these results to those of Figure 13, it is apparent that the narrower source will require a more severe time step interval limit than the broader source.

The results have demonstrated time step interval limitations when areal sources are present. If the source strength

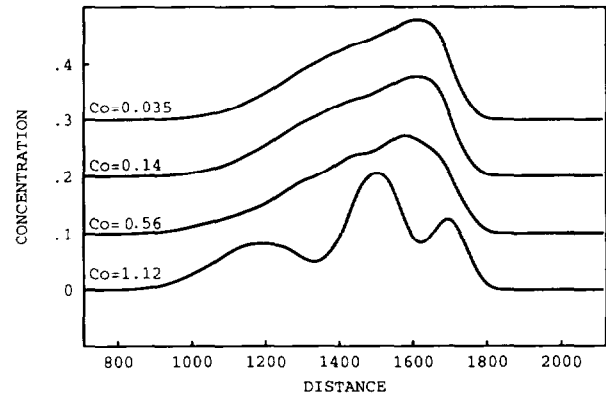


Fig. 15. Concentration profiles, contaminated soil problem. Concentration profiles along the streamline that passes through a one-node source are shown for four Crank-Nicolson solutions at time 32 years. Starting at the top, time step increments were $\Delta t = 0.5$ year ($Co = 0.035$), $\Delta t = 2$ years ($Co = 0.14$), $\Delta t = 8$ years ($Co = 0.56$) and $\Delta t = 16$ years ($Co = 1.12$).

is dependent on background concentration, time truncation errors lead to mass errors in the solutions. The size of the errors will depend on how rapidly the background concentration is changing with time. The time step limitation is significantly less stringent for the Crank-Nicolson formulation than for the implicit formulation. A second limitation arises if the length of backtracks becomes large compared to the length of areal sources. As a general rule, the Lagrangian spatial resolution parameter $\Delta x_L = Co\Delta x$, should be less than some fraction of the characteristic length of the source area or distortions will be generated in the concentration field. For a given Δx , the limits on Δx_L lead to limits on Δt . It should be noted that the Courant number limitations are localized to the source area. In these examples, the significantly larger Courant numbers that occur as the river in the southwest is approached are not limiting factors.

CONCLUSION

The ELLESCO method can be used effectively to solve vertically averaged groundwater transport problems. The effective range of spatial and temporal discretizations is expanded by ELMs, but the character of the approximation errors changes due to the backtracking Lagrangian step in the solution procedure.

To decouple the time truncation error of the tracking step from the time step size of the transport step, a numerical tracking algorithm consisting of a sequence of second-order Runge-Kutta numerical integration steps is presented. The number of Runge-Kutta steps contained in a transport time step interval is adjusted for each collocation point to assure that the accuracy of the final integration meets a specified tolerance. In this manner, the accuracy of the Lagrangian step is independent of the size of the transport time step interval, Δt .

A second-order Runge-Kutta algorithm is used in order to avoid additive errors associated with first-order Euler algorithms. Tracking difficulties near injection wells are overcome by creating capture zones which are delineated by forward tracking. When a collocation point is captured or intersects a domain boundary, an estimate of the time that the flow line has spent in the domain, Δt_i , is made. This

estimate can then be used to adjust the strength of dispersion and source terms in the collocation point's residual. The approach is efficient when the size of the time step and the complexity of the velocity field are such that the majority of the collocation point tracks converge in two or four Runge-Kutta steps. When a large percentage of the collocation point tracks take eight or more Runge-Kutta steps to converge, the algorithm becomes less efficient, because the number of discarded preliminary calculations increases.

When the velocity field is accurate, ELLESCO combined with numerical tracking has good global mass balance and accurate front propagation characteristics. However, velocity errors due to errors in the numerical solution of the flow equations can lead to global mass balance errors as well as inaccurate positioning of the front.

The example calculations have also identified limits to the spatial and temporal discretizations. Sharp fronts can be accurately represented as long as they are spread over a minimum of one and a half ELLESCO elements. If the length of a front is less than one and a half elements, oscillations develop. This limit is due to the Eulerian spatial discretization.

Previously reported ELM results have not contained areal sources, and the results in these works indicated that the upper limit on Δt was quite large for advective-dominated flow. They also indicated that the advantages of the Crank-Nicolson formulation over the implicit formulation were not generally worth the added computational effort. This conclusion was reached because dispersion is small in an advective-dominated transport system, so time truncation errors from the first-order implicit discretization of the dispersion terms will not be large.

The addition of the areal source terms leads to more stringent limits on Δt . If the source strength is dependent on the local concentration in the aquifer and the concentration is changing with time, then time truncation errors associated with the source terms lead to mass balance errors. The effective limit on Δt depends on how rapidly the aquifer concentration is changing with time. The limit on Δt is dramatically relaxed when the Crank-Nicolson scheme is used. The main disadvantage of the Crank-Nicolson formulation is the necessity of computing dispersion term spatial derivatives of the concentration at the back projected locations. An efficient approach is to use the implicit discretization for dispersion and Crank-Nicolson for source terms.

A Lagrangian spatial resolution parameter is defined as $\Delta x_L = Co\Delta x$. It is indicative of the distance between the head and foot of a characteristic, and it is an indicator of the size of spatially fixed features that can be resolved. In the vicinity of a fixed source, the value of Δx_L must be less than the length of the source, or distortions will arise in the concentration field. Limits on Δx_L translate into limits on

Δt , because of the dependence of Δx_L on the Courant number.

Acknowledgments. We wish to acknowledge support from the Air Force Office of Scientific Research, Bolling AFB, D. C., and Department of Energy grant DE FG02-86ER60453.A004, Subsurface Science Program, Office of Basic Energy Research.

REFERENCES

- Baptista, A. E., E. E. Adams, and K. D. Stolzenbach, Eulerian-Lagrangian analysis of pollutant transport in shallow water, *Rep. 296*, Ralph M. Parsons Lab., Mass. Inst. of Technol., Cambridge, 1984.
- Bentley, L. R., and G. F. Pinder, Eulerian-Lagrangian least squares collocation in multi-spatial dimensions, in *Computational Methods in Geoscience*, vol. 1, pp. 111-141, Society for Industrial and Applied Mathematics, Philadelphia, Pa., 1992.
- Bentley, L. R., G. F. Pinder, and I. Herrera, Solution of the advective-dispersive transport equation using a least squares collocation, Eulerian-Lagrangian method, *Numer. Methods Partial Differ. Equations*, 5, 227-240, 1989.
- Bentley, L. R., A. Aldama, and G. F. Pinder, Fourier analysis of the Eulerian-Lagrangian least squares collocation method, *Int. J. Numer. Methods Fluids*, 11, 427-444, 1990.
- Cheng, R. T., V. Casulli, and S. N. Milford, Eulerian-Lagrangian solution of the convection-dispersion equation in natural coordinates, *Water Resour. Res.*, 20, 944-952, 1984.
- Chiang, C. Y., M. F. Wheeler, and P. B. Bedient, A modified method of characteristics technique and mixed finite elements method for simulation of groundwater solute transport, *Water Resour. Res.*, 25, 1541-1549, 1989.
- Glass, J., and W. Rodi, A higher order numerical scheme for scalar transport, *Comput. Meth. Appl. Mech. Eng.*, 31, 337-358, 1982.
- Holly, F. M., Jr., and J.-M. Usseglio-Polatera, Dispersion simulation in two-dimensional tidal flow, *J. Hydraul. Eng.*, 110, 905-926, 1984.
- Javandel, I., C. Doughty, and C. F. Tsang, *Groundwater Transport: Handbook of Mathematical Models*, *Water Resour. Monogr. Ser.*, vol. 10, AGU, Washington, D. C., 1984.
- Komatsu, T., F. M. Holly, Jr., N. Nakashiki, and K. Ohgushi, Numerical calculation of pollutant transport in one and two dimensions, *J. Hydraul. Eng.*, 3, 15-30, 1985.
- Neuman, S. P., Adaptive Eulerian-Lagrangian finite element method for advection-dispersion, *Int. J. Numer. Methods Eng.*, 20, 321-337, 1984.
- Pinder, G. F., and W. G. Gray, *Finite Element Simulation in Surface and Subsurface Hydrology*, Academic, San Diego, Calif., 1977.
- Zihuhua, O., and D. Elsworth, An adaptive characteristics method for advective-diffusive transport, *Appl. Math. Modell.*, 13, 682-692, 1989.
- L. R. Bentley, Department of Geology and Geophysics, University of Calgary, 2500 University Drive N.W., Calgary, Alberta, Canada T2N 1N4.
- G. F. Pinder, College of Engineering and Mathematics, University of Vermont, Burlington, VT 05405.

(Received August 5, 1991;
revised June 19, 1992;
accepted July 15, 1992.)